3838 *Biochemistry* **2009,** *48,* 3838–3846
DOI:10.1021/bi900144a

BIOCHEMISTRY
including biophysical chemistry & molecular biology
Accelerated Publication

Role for Threonine 201 in the Catalytic Cycle of the Soluble Diiron Hydroxylase Toluene 4-Monooxygenase[†,‡]

Nathaniel L. Elsen, Lucas J. Bailey, Andrew D. Hauser, and Brian G. Fox*

Department of Biochemistry, College of Agricultural and Life Sciences, University of Wisconsin, Madison, Wisconsin 53706-1544

Received January 28, 2009. Revised Manuscript Received March 4, 2009

ABSTRACT: The active site residue Thr-201 in toluene 4-monooxygenase hydroxylase (T4moH) has a structural counterpart in the active sites of all diiron monooxygenases. Thus, our previous finding that mutation of this residue to Ala, Gly, or Ser had no impact on steady-state catalysis or coupling was surprising. In this work, we provide kinetic, biochemical, and structural evidence that one role of Thr-201 may be to stabilize a peroxo-level intermediate during enzyme catalysis. During reactions in the absence of substrate, T201 T4moH slowly consumed O_2 but only a negligible amount of H_2O_2 was released. In contrast, T201A T4moH gave stoichometric release of H_2O_2 during reaction in the absence of substrate. Both enzyme isoforms were tightly coupled during steady-state catalysis with saturating toluene and other optimal substrates and exhibited near-identical kinetic parameters. However, rapid mix single-turnover studies showed that T201A T4moH had a faster first-order rate constant for product formation than T201 T4moH did. Comparison of X-ray crystal structures of resting and reduced T201A T4moH in complex with T4moD with comparable structures of T201 T4moHD revealed changes in the positions of several key active site residues relative to the comparable structures of T201 T4moH with T4moD. This combination of catalytic and structural studies offers important new insight into the role of the role of conserved Thr-201, and its contributions to the catalytic reaction cycle.

Soluble diiron monooxygenases catalyze the NADH- and O_2-dependent oxidation of aliphatic and aromatic organic substrates as the first step of a metabolic pathway that can supply the total carbon and energy needs of the host bacterium (*1*−*3*). Many of these multicomponent enzymes, including methane monooxygenase (MMO),[1] toluene/*o*-xylene monooxygenase (ToMO), and toluene 4-monooxygenase (T4MO), have been studied in vitro (*4*−*6*), and the most extensively characterized of these is MMO (*7*,*8*). The catalytic cycle of MMO begins with two-electron reduction of the diferric center (*9*). The diferrous center reacts with O_2 to form an initial Michaelis complex (*10*), followed by rapid reaction to form compound P, a diferric peroxo species in which the peroxo O atoms are thought to bind in a relatively symmetric μ-1,2 bridging mode (*11*). Compound P decays to form compound Q, an oxo-bridged diferryl species responsible for hydroxylation of methane (*12*). Compounds P and Q have distinctive spectroscopic features that have facilitated detailed transient kinetic studies of their reactions (*10*−*12*). A peroxo species similar to compound P was observed in the mouse ribonucleotide reductase R2 component as a precursor to intermediate X, a Fe(III)−Fe(IV) mixed valence reactive species (*13*). Ferritin also produces a reactive peroxo species during iron deposition (*14*), and stearoyl-ACP Δ^9 desaturase yields a quasi-stable peroxo intermediate [$t_{1/2} \sim 30$ min (*15*)] that decays to a resting diferric state without desaturating the fatty acid.

Toluene 4-monooxygenase (T4MO) from *Pseudomonas mendocina* KR1 catalyzes the hydroxylation of toluene to form *p*-cresol (*5*). Unlike the radical rebound (*16*−*18*) or concerted oxygen insertion (*19*) mechanisms favored for hydroxylation of methane and other alkanes,

*To whom correspondence should be addressed: Department of Biochemistry, 433 Babcock Dr., University of Wisconsin, Madison, WI 53706. Phone: (608) 262-9708. Fax: (608) 262-3453. E-mail: bgfox@biochem.wisc.edu.

†This work was funded by National Science Foundation Grant MCB-0316232 to B.G.F. Use of the Advanced Photon Source was supported by the U.S. Department of Energy, Basic Energy Sciences, Office of Science, under Contract W-31-109-ENG-38. Use of the Life Science Collaborative Access Team beamlines at the Advanced Photon Source was supported by the College of Agricultural and Life Sciences, Department of Biochemistry, and Graduate School of the University of Wisconsin.

‡Coordinates and structure factors have been deposited in the Protein Data Bank (PBD) as entries 3GE8 (resting T201A T4moHD complex) and 3GE3 (reduced T201A T4moHD complex).

[1]Abbreviations: MMO, methane monooxygenase; MmoH, MMO hydroxylase component; ToMO, toluene/*o*-xylene monooxygenase; ToMOH, ToMO hydroxylase; T4MO, four-protein toluene 4-monooxygenase complex from *Pseudomonas mendocina* KR1; T4moH, hydroxylase component of T4MO; T4moC, Rieske-type [2Fe-2S] component of T4MO; T4moD, effector protein of T4MO; T4moF, oxidoreductase component of T4MO.

Published on Web 3/16/2009

hydroxylation of aromatic substrates by T4MO and other four-component alkene/aromatic monooxygenases likely proceeds by electrophilic aromatic substitution (*20*,*21*). However, despite the significant body of published work describing the steady-state and transient kinetics of the soluble diiron monooxygenases, certain aspects regarding the reactivity of the diiron cofactor with O_2 and organic substrates remain unexplained. These include the role of a threonine residue comparable to Thr-201 of T4moH that is strictly conserved among soluble diiron monooxygenases although not required for steady-state catalysis (*22*) and the nature of reactive diiron intermediates used in the aromatic ring monooxygenases like T4moH and ToMOH. Except for an unusual peroxo species with no visible chromophore recently identified in ToMOH (*21*,*23*), no diiron species comparable to compounds P and Q of MMO have been reported for the aromatic ring monooxygenases, despite substantial similarities in their active sites.

In this work, new insights into T4moH reactivity were gained from a combination of steady-state and transient kinetic experiments and X-ray crystallographic studies. Surprisingly, Thr-201 of T4moH slows the first-order rate constant for product formation as compared to a mutant containing Ala at that position. However, this slowed reaction corresponds to efficient retention of a peroxide-level oxidizing species on the enzyme in the absence of substrate. In contrast, T201A T4moH has a faster rate of single-turnover product formation with all substrates tested yet readily releases H_2O_2 in the absence of substrate. This profound difference in the ability to retain a peroxide-level oxidizing species would significantly impact the coupling efficiency at nonsaturating concentrations of toluene. Thus, Thr-201 may be conserved due to this major impact on diiron monooxygenase function. The crystal structures of the resting and reduced T201A T4moH isoform in complex with T4moD showed that changes associated with the mutagenesis were localized to the active site and influenced the positioning of key residues along helix αE, including diiron center ligands E197 and E231. In conjunction, these kinetic and structural studies of T201A T4moH offer important new insight into the role of conserved Thr-201 during T4moH catalysis.

MATERIALS AND METHODS

Materials. Substrates, products, and other chemicals were from Aldrich (Milwaukee, WI). The preparations of the T4MO proteins were as previously reported (*5*,*24*−*27*).

Catalytic Assays. Steady-state reactions of the reconstituted T4MO complex were assessed as previously described (*28*) except the assays were performed at 4 °C. Coupling reactions were performed with the same protein component concentrations as the steady-state activity assays, initiated by the addition of NADH (typically 250 μM), and allowed to go to completion before total products were analyzed. Steady-state O_2 consumption was monitored using a Clark-type oxygen electrode (Hansatech Instruments, Norfolk, England). The electrode was calibrated with 10 units of 3,4-protocatechuate dioxygenase (Sigma) and 100 μM protocatechuic acid (*29*). The total reaction volume was 1 mL, and the following protein concentrations were used: 0.5 μM T4moH (active sites), 4 μM T4moD, 3 μM T4moC, and 0.1 μM T4moF. Hydrocarbon substrate was added to a final concentration of 1 mM, and the reaction was initiated by the addition of 500 μM NADH. For studies with no substrate, 4 μM T4moH (active sites), 4 μM T4moD, 3 μM T4moC, and 0.1 μM T4moF were used. T4MO components tested for catalase activity were combined in 1 mL of reaction buffer, and the reaction was initiated by addition of 50 mM peroxide calibrated by its absorbance at 240 nm (ε = 43.6 M^{-1} cm^{-1}). Reactions containing added catalase (1000 units, Sigma), superoxide dismutase (10 units, Sigma), and peroxidase (10 units, Sigma) were assayed using the oxygen electrode. Horseradish peroxidase assays of the rate and stoichiometry of H_2O_2 formation were performed with 2,2′-azinobis(3-ethylbenzthiazoline-6-sulfonic acid) (*30*).

Single-Turnover Reactions. The rate of product formation in a single-turnover reaction was determined by rapid-mix chemical quench. Protein stocks were mixed in the appropriate ratios, made anaerobic by vacuum/argon cycling in a septum-sealed vial, transferred into an anaerobic chamber (Coy Laboratory Products Inc., Grass City, MI), and reduced by stoichiometric addition of NADH relative to T4moH active sites. While still in the glovebox, the reduced samples were transferred into a syringe for the rapid-mix chemical quench device (Update Instruments, Madison, WI). A second syringe was prepared by bubbling 100% O_2 through 10 mL of 50 mM phosphate (pH 7.5) containing 50 mM NaCl in a 15 mL Falcon tube. An aliquot (10 μL) of the substrate was added to the oxygenated reaction buffer. This solution was transferred to the second rapid-mix syringe. Both syringes were then transferred to the rapid-mix device and maintained at 4 °C throughout the experiment. Aging hoses were prechilled and also maintained at 4 °C. During the rapid-mix experiments, reactions (100 μL) were quenched at the times specified after mixing by direct injection into 150 μL of a 2 N HCl/saturated NaCl solution. Products were quantified by gas chromatography as previously described (*28*), and rate constants and amplitudes were determined by least-squares fitting of the data with a single exponential (Sigma-Plot, Point Richmond, CA).

Crystallographic Methods. Conditions and methods for structure determination were identical to those previously reported for the oxidized and reduced wild-type T4moHD complex (*27*). Diffraction data for the resting complex were collected at LS-CAT beamline 21-ID-G, and diffraction data for the reduced complex were collected at LS-CAT beamline 21-ID-D at the Advanced Photon Source (Argonne National Laboratory, Argonne, IL). The data were indexed, integrated, and scaled by using HKL2000 (*31*). The structures of the resting and reduced T201A T4moHD complexes were determined by molecular replacement with the CCP4 suite program MOLREP (*32*) using 3DHH as the starting model. An initial round of simulated annealing was performed in PHENIX (*33*). Electron density was fit and refined by repeated cycles using Coot (*34*) and REFMAC5 (*35*). Ramachandran and rotamer analyses were performed with Molprobity (*36*). Figures were prepared with PyMOL (*37*).

Table 1: Rate Constants and Coupling Efficiencies in Single-Turnover and Steady-State Reactions of T4moH Isoforms at 4 °C

		T4moH			T201A T4moH		
	substrate	rate constant (s^{-1})	coupling efficiency[c] (%)	effective rate[d]	rate constant (s^{-1})	coupling efficiency[c] (%)	effective rate
single turnover[a]	NO_2-benzene	0.11 (0.01)	16.5 (0.3)		0.31 (0.01)	17.3 (0.3)	
	Cl-benzene	0.91 (0.02)	40.0 (0.4)		3.8 (0.2)	24 (0.6)	
	benzene	1.9 (0.2)	101 (4)		8.5 (0.8)	102 (5)	
	toluene	2.0 (0.1)	95 (1)		8.5 (0.2)	95 (1)	
	anisole	0.89 (0.02)	97 (1)		5.9 (0.2)	97 (1)	
steady state[b]	NO_2-benzene	0.013 (0.001)	12 (2)	0.11	0.034 (0.002)	21 (1)	0.16
	Cl-benzene	0.075 (0.006)	39 (1)	0.19	0.087 (0.002)	34 (3)	0.26
	benzene	0.10 (0.01)	98 (2)	0.10	0.31 (0.01)	101 (3)	0.31
	toluene	0.21 (0.02)	94 (2)	0.22	0.23 (0.01)	97 (2)	0.24
	anisole	0.16 (0.02)	87 (4)	0.18	0.23 (0.01)	100 (10)	0.23

[a] For single turnover, the rate constant was obtained from fitting rapid-mix chemical quench time points to a single-exponential equation. [b] For steady state, the rate constant reported was k_{cat} for product formation at 4 °C. [c] For single turnover, coupling efficiency was calculated from the molar ratio of products observed to diiron sites present. For steady state, coupling efficiency was calculated from the molar ratio of products observed to NADH added. [d] The effective rate of active site turnover leading to product after accounting for uncoupled reactions was calculated as (rate constant)/(percent coupling) × 100.

RESULTS

Single-Turnover Kinetics of T4moH and T201A T4moH. Calculated rate constants and amplitudes for all single-turnover experiments are listed in Table 1. T4moH had a single-turnover product formation rate constant of ~2 s^{-1} at 4 °C with saturating toluene as substrate and gave a near-stoichiometric yield of *p*-cresol product. Figure 1A shows product formation time courses for various substrates during single-turnover reactions. The product formation rate constants measured for the different substituted benzenes did not exhibit a linear dependence on the predicted electronic effects of the substituent (*38*). Moreover, the product formation rate constants did not correlate with the coupling efficiency for a given substrate. For instance, anisole (0.91 s^{-1}) and Cl-benzene (0.89 s^{-1}) were converted to product at the same rate in the single-turnover reactions, but anisole was fully coupled (97% product yield) and Cl-benzene only weakly coupled (40% product yield), which was reflected in the amplitude of the reactions. In general, the amplitude of the single-turnover reaction (coupling efficiency) increased with the predicted electron donating ability of the substituent and was maximized at ~100% with benzene, toluene, and anisole. O_2 consumption assays gave insight into a mechanism for this (see below). Figure 1B shows the results of single-turnover reactions of T201A T4moH. The mutated enzyme gave product yields similar to that of T4moH at a saturating substrate concentration. However, and surprisingly, the single-turnover product formation rate constants for the mutated enzyme were 3−6 times faster for every substrate tested (Table 1).

Steady-State Product Formation and Coupling. Table 1 lists results from steady-state catalysis. These experiments were performed at 4 °C to permit direct comparison with the single-turnover studies. Upon accounting for the difference in temperature, we found these results were consistent with rates previously reported for oxidation of these substrates by both T201 T4moH and T201A T4moH (*22*,*28*). The steady-state and single-turnover coupling efficiencies were similar (Table 1). The observed steady-state product appearance rate determined by gas chromatography reflects only the productive consumption of O_2 and NADH. Normalization of the observed steady-state rate with the coupling efficiency yielded the effective steady-state turnover rate. Comparison of the rates for the single-turnover reactions and effective steady-state turnover rates (Table 1) revealed that for every substrate except NO_2-benzene, the single-turnover product formation rate was ~5−20-fold faster than the

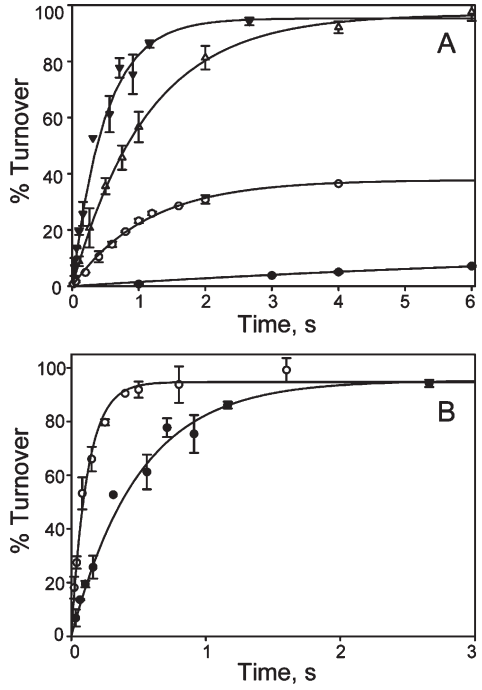

FIGURE 1: Rapid-mix chemical quench single-turnover reactions of T201 T4moH and T201A T4moH. After being mixed, the reaction mixtures contained 100 μM diiron sites, 100 μM T4moC, and 100 μM T4moD. The percent turnover amplitude includes contributions from all observed product isomers. Product distributions were similar to those previously reported in steady-state catalysis (*22*,*28*). (A) Single-turnover reactions of T201 T4moH with NO_2-benzene (●), Cl-benzene (○), toluene (▼), and anisole (△). (B) Comparison of the single-turnover reactions of T201 T4moH (●) and T201A T4moH (○) with toluene.

effective steady-state rate. For instance, while the single-turnover product formation rate with Cl-benzene was 0.89 s^{-1}, combination of the steady-state rate of chlorophenol formation, 0.075 s^{-1}, and the coupling efficiency, 39%, indicated that the active site was turning over O_2 and NADH to generate product at an effective rate of 0.2 s^{-1}.

For NO_2-benzene, the observed steady-state turnover rate (0.013 s^{-1}) and coupling efficiency (12%) yielded an effective steady-state turnover number of 0.11 s^{-1}. This matched the single-turnover rate for nitrophenol formation (Table 1). Thus, NO_2-benzene was the only substrate tested in which product formation appeared to be rate-determining for the overall catalytic cycle.

Peroxide Consumption. A catalase activity has been reported for T4moH and ToMOH (*5*,*21*,*39*). Azide (100 mM) inhibited the catalase activity present in T4moH without decreasing the activity of the enzyme for toluene hydroxylation. This catalase activity did not correlate closely with active site concentration and was not changed by the addition of either T4moC or T4moD. Furthermore, addition of hydroxylamine (20 μM), another potent inhibitor of *Escherichia coli* catalase (*40*), decreased the catalase activity by >95% without affecting toluene hydroxylation activity. These results suggest that the observed endogenous catalase activity was from a contaminant, not from T4moH.

O_2 Consumption Assays in the Absence of Substrate. Table 2 lists the rates of O_2 consumption with various substrates and components of T4MO. Hydroxylamine (20 μM) was included in all O_2 consumption assays except those to which exogenous catalase (1000 units) was added. In the presence of excess exogenous catalase, a decrease in the rate of O_2 consumption would correspond to the stoichiometry of the catalase reaction ($2H_2O_2 \rightarrow 2H_2O + O_2$) and thus provide a method for quantifying the amount of H_2O_2 released from an enzyme (*41*).

The electron transfer components T4moC and T4moF consumed O_2 at a rate near the error associated with baseline drift of the O_2 electrode, 0.005 s^{-1}. Addition of catalase reduced this rate by ~40%, indicating that a low level of H_2O_2 might be produced by the electron transfer components, and indeed, horseradish peroxidase-catalyzed dye oxidation confirmed this. In the absence of substrate, the fully reconstituted T4MO system containing T4moH, T4moD, T4moC, and T4moF consumed O_2 at a rate of 0.018 s^{-1}. When catalase was added to this reaction mixture, the O_2 consumption rate was decreased to 0.013 s^{-1}. Because of the overall low rates measured, the error associated with electrode drift, and the presence of T4moF and T4moC in the reaction mixture, the conclusion that T4moH releases H_2O_2 in the absence of substrate is equivocal. In contrast, the reconstituted T201A T4moH system consumed O_2 at a rate of 0.168 s^{-1}, and addition of catalase reduced this rate to 0.085 s^{-1}. After accounting for O_2 potentially consumed by T4moC and T4moF, we found the rate of O_2 consumption observed in the presence of T201A T4moH was ~10-fold higher than that observed with T4moH. Furthermore, the 50% decrease in rate observed in the presence of catalase indicated that nearly all of the O_2 consumed could be identified as H_2O_2 released from the mutated enzyme. Dye oxidation experiments using horseradish peroxidase confirmed both the increased rate and the stoichiometry of release of H_2O_2 from T201A T4moH.

O_2 Consumption Assays with Substrate Present. Addition of a saturating amount of toluene to fully reconstituted T4MO increased the steady-state O_2 consumption rate by ~100-fold relative to active site concentration, and the reactions were fully coupled [Table 2 (*25*,*28*)]. Interestingly, the combination of the steady-state product formation rate and coupling efficiency suggested that when T4moH reacted with Cl-benzene, toluene, or anisole (Table 1) to give hydroxylated products, the active site turned over at a similar effective rate. This was confirmed by monitoring O_2 consumption (Table 2). The high level of uncoupling observed with Cl-benzene raised the question of the fate of the majority of the O_2 consumed. Addition of catalase to the reaction mixtures containing saturating Cl-benzene (1 mM) did not reduce the rate of O_2 consumed by either T4moH or T201A T4moH, indicating that uncoupling in the presence of substrate was not caused by release of H_2O_2 (note that catalase was not inhibited by Cl-benzene at the concentrations used here). Likewise, addition of superoxide

Table 2: O_2 Consumption Rates Determined for T4moH Isoforms at 20 °C

		O_2 consumption rate[c] (s^{-1})	
protein components	substrate[a]	T4moH	T201A T4moH
T4moH isoform, T4moC, T4moD, T4moF	none	0.018[d]	0.168
	with catalase[b]	0.013	0.085
T4moH isoform, T4moC, T4moD, T4moF	toluene	2.2	2.0
	anisole	2.0	nd[e]
	benzene	1.4	2.0
	Cl-benzene	2.0	2.0
	with catalase	2.0	2.0
	NO_2-benzene	0.6	0.8
	with catalase	0.4	0.6

[a] Substrate was added to a final concentration of 1 mM when indicated. Previous studies (*28*) established this concentration was saturating in steady-state catalysis for all substrates tested. [b] One thousand units of catalase added. [c] Corrected for contributions from electron transfer components and normalized for T4moH active site concentration (see Materials and Methods). [d] The error in the measurement associated with baseline drift of the O_2 electrode was ~0.005 s^{-1} under these assay conditions and is included in all reported values. [e] Not determined.

dismutase did not affect the O_2 consumption rate. Furthermore, substrates for which no product could be detected, such as phenol and aniline, also stimulated a large increase in the rate of O_2 consumption that was not altered by addition of catalase or superoxide dismutase. These results indicate that substrate binding may stimulate O_2 consumption without completion of the hydroxylation reaction. Moreover, in the case of T201A T4moH, the presence of substrate completely suppressed the release of H_2O_2 from the enzyme. Possible mechanisms for how this may occur are considered in Discussion.

Crystal Structures of Resting and Reduced T201A T4moH−T4moD Complexes. Table S1 of the Supporting Information lists statistics from the crystallization and structure determinations. The crystal structure of T201 T4moH in complex with T4moD (T201A T4moHD) was determined in both the resting and sodium dithionite-reduced states. In the resting state, the complex crystallized in the $P2_12_12_1$ space group and the asymmetric unit contained the functional dimer of the TmoA, TmoB, and TmoE polypeptides of T4moH along with 2 mol of T4moD. In the reduced form, the complex crystallized in the $C222_1$ space group and the asymmetric unit was a single protomer.

Overall, the resting and reduced T201A T4moHD structures were remarkably similar to the T201 T4moHD structures (*27*). The α-carbons of the TmoA polypeptides containing the active sites in the resting T201A and T201 T4moHD complexes aligned with a root-mean-square deviation (rmsd) of 0.20 Å, while the reduced forms aligned with a rmsd of 0.14 Å. Despite this overall similarity, there were notable differences at the active site.

To review the key features of the resting T201 T4moHD structure (*27*), the Fe−Fe distance was 3.3 Å, the hydroxyl group of T201 hydrogen bonded to a carboxylate oxygen of the diiron ligand E231, and the methyl group of T201 positioned the side chain of F196 above the active site. Three water/hydroxo molecules were identified in resting T201 T4moHD: HOH2 was a bridge between the Fe atoms; HOH3 was bound to Fe1; and HOH5 was positioned by HOH3 and the side chains of Q228 and E231. HOH5 was not present in the T4moH structure lacking T4moD (*27*).

Figure 2A shows the models for active site regions of the resting T201 T4moHD (light blue) and T201A T4moHD (white). The loss of the hydrogen bonding contact in the T201A structure led to an elevated *B* value for the carboxylate group of E231 as compared to the *B* values of the other active site residues. The T201A mutation also led to changes in TmoA helix αE (see Figure S1 of the Supporting Information), which extended from A185 to E214 and included the diiron ligand E197. From T193 to F196, the Cα positions varied by up to 2.5 Å and rotamer flips were observed in residues F194 and S195. Furthermore, in response to the loss of the methyl group in the T201A T4moHD active site, the side chain of F196 shifted ~2 Å closer to the diiron center. The Fe−Fe−OE1 angle of E197 increased by ~10° in resting T4moHD and T201A T4moHD as compared to that in resting T4moH (see Figure S2 of the Supporting Information).

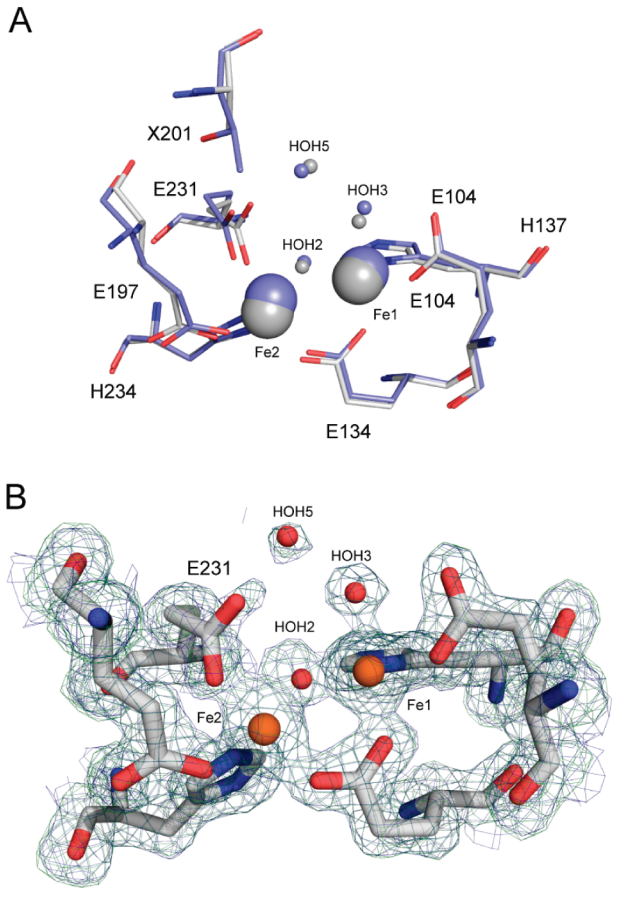

FIGURE 2: Models for the active site of T201A T4moH in complex with T4moD. (A) Resting T201 T4moHD [light blue, 1.9 Å (*27*)] compared to resting T201A T4moHD (white, 2.2 Å). Active site residues are labeled. The positions of the iron atoms and three active site water molecules (HOH2, HOH3, and HOH5) are also indicated. The positions of the side chains of Fe2 ligands E197 and E231 are altered slightly in the mutated enzyme. The positions of other iron ligands are indistinguishable. (B) Active site model for reduced T201A T4moH and $F_o - F_c$ (slate) and $2F_o - F_c$ (green) electron density maps (1.5 Å). In reduced T201A T4moHD, the Fe−Fe distance showed the same increase to 3.4 Å observed in reduced T201 T4moHD and HOH2, HOH3, and HOH5 were also retained. The Fe2 ligand E231 did not assume a bridging position in the mutated enzyme, representing a major structural difference. T201A T4moHD has an ~3−6-fold faster rate of single-turnover catalysis than T201 T4moHD with all substrates tested.

In the reduced T201 T4moHD structure, the Fe−Fe distance was 3.4 Å (*27*), and the E231 carboxylate group rotated away from T201 and displaced the water molecule bridging between the iron atoms. This gave a rearranged structure with one carboxylate oxygen atom from E231 ligated to Fe2 and the other carboxylate oxygen bridging both Fe atoms. Figure 2B shows the model and electron density map of E231 in the reduced T201A structure, while Figure S2 of the Supporting Information shows the positions of E197 and E231 in reduced T4moHD and reduced T201A T4moHD. Significantly, the change in coordination mode observed for E231 in the reduced T201 T4moHD structure was not observed in the T201A structure. However, despite the absence of this new bridging moiety, the Fe−Fe distance in the T201A T4moHD structure increased to 3.4 Å, which was observed upon reduction of T201 T4moHD. The Fe−Fe−OE1 angle of E197 increased by ~5° in reduced T201A

T4moHD as compared to that in reduced T4moHD (see Figure S2 of the Supporting Information). In both the resting and reduced T201A T4moHD structures, active site water/hydroxo molecules HOH2, HOH3, and HOH5 were observed.

DISCUSSION

Stearoyl-ACP Δ^9-desaturase has a Thr residue in the active site that is structurally analogous to Thr-201 in T4moH (*42*). Mutation of this residue to Ala eliminated desaturase activity and converted the enzyme into a peroxidase ($H_2O_2 + 2e^- + 2H^+ \rightarrow 2H_2O$), providing insight into one possible role of this residue in diiron enzymes. This work and previous studies have shown that T201 T4moH and T201A T4moHD are functionally equivalent in steady-state catalysis. However, T201A T4moH exhibited faster single-turnover catalysis than T201 T4moH. Furthermore, T201A T4moH readily released peroxide in the absence of substrate. Cytochrome P450s also have an active site Thr residue. Mutation of Thr-252 to Ala in P-450$_{CAM}$ caused uncoupling with release of H_2O_2 and profound loss of hydroxylation activity, and the crystal structure showed a solvent molecule had occupied the O_2 binding site (*43*). In complex with T4moD, T201A T4moH retained the active site waters present in the unmodified enzyme, reflecting the importance of the effector−hydroxylase complex in setting the active site configuration for catalysis. Unlike the P450 mutation, T201A T4moH also retained full, regiospecific hydroxylation activity in the presence of a saturating amount of substrate. In the following, we discuss how this combination of results might arise and the potential consequences for the enzyme reaction.

Model of Diiron Center Turnover. Figure 3 shows a scheme for diiron center catalysis. This discussion presumes that similar metal-bound intermediates are formed upon reaction of diferrous sites with O_2 in both the presence and absence of substrate, and this is supported by studies of reaction intermediates of MMO and ToMO (*10*,*21*,*23*,*44*−*46*). Upon reaction of the Michaelis-type complex of a diferrous center and O_2 ($E^{2+}-O_2$, k_1), the active site presumably contains a diferric center bound to an O_2-derived species at the peroxide oxidation level (E^{3+}−peroxo). This species may be analogous to the species observed in ToMOH by Mössbauer spectroscopy (*12*). E^{3+}−peroxo may potentially decay by three routes: O−O bond cleavage (k_3) leading to the formation of E^{4+}−oxo, release of H_2O_2 (k_9) to restore resting E^{3+}, or direct (k_{11}) or indirect (k_{13}) reductive quenching. With substrate present, either E^{4+}−oxo (k_5) or E^{3+}−peroxo (k_7) may potentially react to give product, in addition to uncoupling reactions k_9, k_{11}, and k_{13}.

In MmoH, compound P formed at ~20 s^{-1}, and this step was pH-dependent (*10*,*44*) Conversion from compound P to compound Q (E^{4+}−oxo) occurred at a rate of 1.2 s^{-1} and was insensitive to the presence of substrate; this step was also pH-dependent. Compound Q reacted with methane at 19000 M^{-1} s^{-1} (*10*) and norcarane at 0.53 s^{-1} (*45*); compound P oxidized ethers (*46*).

Recently, an unusual peroxo species with no chromophore in the visible region and a Mössbauer isomer shift

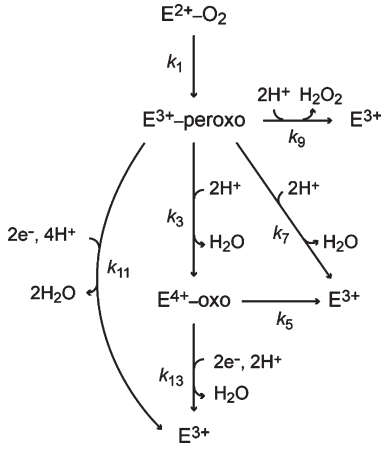

FIGURE 3: Schematic representation of the T4moH reaction cycle considered in Discussion. Reactions are assumed to be irreversible. In this scheme, steps k_5 and k_7 indicate reactions with substrate that lead to product formation. Since the kinetic order of substrate addition is at present not known, substrate binding is not explicitly assigned to a single kinetic step in this scheme. However, substrate binding may influence any of the other individual steps shown in the scheme. E^{2+} denotes a diferrous state, E^{3+} a resting diferric state, E^{3+}−peroxo a peroxodiferric state, and E^{4+}−oxo a diferryl state. The rate constant k_1 represents conversion of a Michaelis-type ($E^{2+}-O_2$) complex to E^{3+}−peroxo; k_3 represents conversion of E^{3+}−peroxo to E^{4+}−oxo. The reaction constant k_5 controls product formation via reaction of E^{4+}−oxo when substrate is present, while k_7 controls product formation via E^{3+}−peroxo when substrate is present. Uncoupling may occur by release of H_2O_2 (k_9), reduction of E^{3+}−peroxo (k_{11}), or reduction of E^{4+}−oxo (k_{13}).

similar to the resting enzyme was proposed to be the oxidizing intermediate in ToMOH (*21*,*23*). This species was detected by Mössbauer spectroscopy in rapid-mix freeze quench samples. Murray and co-workers concluded that this colorless species was responsible for arene hydroxylation because its decay rate increased when substrate was included in the reaction.

The results in Tables 1 and 2 show that both the T4moH active site residues and the presence or absence of substrates influence H_2O_2 release (k_9) and reductive quenching (either k_{11} or k_{13}). Notably, our coupling studies have shown that the presence of substrate can dramatically influence the progress of the reaction cycle, perhaps through alteration of the types, timing, and partition of reaction intermediates. To date, X-ray crystal structures determined for T4moHD have revealed rearrangements of active site ligands caused by T4moD binding, reduction of the diiron center, and the T201A mutation. Should these rearrangements occur during the catalytic cycle, they may represent rate-determining steps that are decoupled from chemical steps of the catalysis.

Release of H_2O_2 by T201A T4moH. In the absence of substrate, T201A T4moH consumed O_2 substantially faster than T201 T4moH, and addition of catalase revealed that nearly all of the O_2 consumed was released as H_2O_2. These results suggest that T201 may help to form or stabilize E^{3+}−peroxo during the T4MO reaction cycle. It might do so directly as a hydrogen-bonding partner to a peroxo moiety bound in the active site or indirectly by stabilizing a water molecule or some other residue that interacts with the peroxo species. Corresponding to the latter possibility, the hydroxyl group of T201 T4moHD is less than 7 Å from Fe2 and plays a central role in the

extensive conformational changes and hydrogen bonding interactions caused by T4moD binding (*27*). The T201 hydroxyl group stabilizes one configuration of Fe2 ligand E231, which in turn helps to localize unique water HOH5 within ~5 Å of the diiron center. It is also possible that the T201 side chain can undergo a rotomer flip during the catalytic cycle to a position more favorable for direct interaction with a diiron intermediate. In T201A T4moH, which reacts faster than T201, the bridging coordination of E231 was not formed in the reduced state. Rearrangement of E231 out of this bridging coordination might represent a required, rate-determining step in diiron enzyme catalysis (*47*). A plausible assignment for this rearrangement step would be either k_1 or k_3, corresponding to conversions among $E^{2+}-O_2$, $E^{3+}-$peroxo, and $E^{4+}-$oxo.

T201 T4moH may release H_2O_2 when substrate is not present, but if so, only a portion of the total O_2 consumed could be identified as H_2O_2 after correction for electrode drift and the uncoupled reactions of the electron transfer components T4moF and T4moC. Therefore, reductive quenching must have consumed the remaining O_2. This would require either direct reduction of $E^{3+}-$peroxo or transient conversion to $E^{4+}-$oxo and then reduction. With regard to reductive uncoupling, peroxoΔ9D was rapidly converted to a resting diferric state in the presence of either sodium dithionite or reduced [2Fe-2S] ferredoxin (*15*), and a similar process is feasible with T4moH. Furthermore, $E^{4+}-$oxo may presumably decay either by reductive quenching (*48*) or possibly by reaction with other buffer substances present in the active site or the polypeptide chain itself.

Despite the increase in the O_2 consumption rate and stoichiometric loss of H_2O_2 observed from T201A T4moH in the absence of substrate, addition of toluene dramatically increased the O_2 consumption rate and gave a stoichiometric yield of hydroxylated product. Thus, the maximal turnover number and complete coupling efficiency were both achieved at a saturating substrate concentration, corresponding to the dominance of substrate hydroxylation k_3k_5 (or k_7) over all other uncoupled pathways for decay of $E^{3+}-$peroxo or $E^{4+}-$oxo.

Substrate-Triggered O_2 Consumption. MmoH displays first-order kinetics in its reaction with methane, a highly diffusible molecule (*10*,*12*). Thus, the slow decay of compound Q allows time for a productive collision with methane that has diffused into the MmoH active site. In contrast, the active site of the T4moHD complex has a shape and size that will bind toluene tightly and specifically (*27*), which possibly allows toluene to participate in the formation and rapid dissipation of reactive intermediates before they can diffuse from the active site or undergo alternative reactions. The ~100-fold stimulation of the rate of O_2 consumption observed in the presence of toluene is consistent with this substrate-dependent enhancement (Table 2). Furthermore, assays using poorly coupled substrates such as Cl-benzene and phenol gave a similar stimulation in the rate of O_2 consumption yet did not stimulate H_2O_2 release and gave only a partial yield of products. Taken together, these results provide strong evidence that the presence of substrate stimulates conversion of early states in the catalytic cycle to more highly reactive intermediates that catalyze substrate hydroxylation or that partition to reductive uncoupling. Precedents for substrate-dependent activation can be found in studies of P450s (*49*) and the 2-His 1-carboxylate family of mononuclear iron enzymes (*50*).

A recent MCD study of the effect of T4moD binding on the T4moH active site, in conjunction with DFT calculations, predicted that the position of the diiron ligand E197 would profoundly influence reactivity toward O_2 (*51*). Specifically, an increase in the Fe−Fe−OE1 angle of E197 was predicted to open a coordination site and orient the HOMO of Fe2 for efficient transfer of an electron to O_2. T4moD binding gave a shift in position of E197 in T4moHD relative to T4moH alone (*27*), and at the resolution presented here, the position of E197 is equivalent in the T201 T4moHD and T201A T4moHD structures (Figure S2 of the Supporting Information). However, the side chain of F196 in T201A T4moHD was shifted by ~2 Å to a position that could potentially be affected by substrate binding. Thus, it is possible that changes in iron ligand E197 are coordinated with substrate binding by interactions along helix αE, including the side chain of F196. This would provide an intriguing but not-yet-demonstrated physical origin for substrate-based activation in T4moHD.

Effects of Substituent on Single-Turnover Rate and Yield. The aromatic ring substituent influenced both the rate and product yield of single-turnover reactions. However, the changes in rate did not linearly correlate with the predicted influence that the different substituents would have on electrophilic aromatic substitution (*38*). For example, anisole was oxidized to methoxyphenol at less than half of the rate at which toluene was oxidized to *p*-cresol despite the predicted stronger ability of a methoxy substituent to stabilize σ-complex formation. As previously mentioned, the presence of substrate stimulated conversion of an early state in the catalytic cycle to more highly reactive intermediates. If this conversion were a rate-determining step, the size and shape of a substituent, more so than electronic effects, might determine the reactivity of a particular substrate. The difference in the size of the methoxy group in anisole versus the methyl group in toluene may introduce unfavorable steric interactions that slow the rate of catalysis but nevertheless still allow for high coupling efficiency and high fidelity for para hydroxylation.

The electronic effects of the substituents were better correlated with coupling efficiency. In this light, it is useful to consider that Cl-benzene and anisole were converted to products with the same rate but with markedly different yields (Table 1). Since no H_2O_2 was observed from either T201 T4moH or T201A T4moH during oxidation of Cl-benzene or toluene, one possibility would be that a rate-determining rearrangement might precede formation of the reactive intermediate $E^{4+}-$oxo. The rearrangement step (k_3) would be sensitive to the steric consequences of substrate binding, accounting for the similar rate of turnover, while the partition between hydroxylation (k_5) and reductive decoupling (k_{13}) would be dependent on the electronic properties of the substrate. Alternatively, the reaction of $E^{3+}-$peroxo (k_7) might be the chemically sensitive step, with uncoupling reactions

provided by $k_3k_5/(k_5 + k_{13}) + k_{11}$. In this alternative mechanism, both size and substituent effects would contribute to the partition between hydroxylation and uncoupled reactions, which complicates further dissection.

Increased Product Formation Rate with T201A T4moH. T201A T4moH had product formation rate constants 3−6-fold higher than that of wild-type T4moH for each of the substrates tested (Table 1), with no difference in product yields. The observed rate increase may have several possible origins. (1) The crystal structure of reduced T201A T4moHD revealed that E231 did not adopt the bridging ligation mode observed in the wild-type structure. It is possible that during turnover of T201 T4moHD the bridging carboxylate oxygen must move out of the bridging position to allow the catalytic cycle to proceed toward formation of reactive intermediates. This rearrangement might represent a rate-determining step that would not be needed in reduced T201A T4moHD. (2) The change in helix αE of the T201A structure may alter the position of F196, E197, or both, with subsequent predicted changes in the reactivity of the diiron center (*51*). (3) A decreased level of stabilization of a peroxo moiety, as evidenced by an increase in k_9 for T201A T4moH (Figure 3), may also increase the rate of formation of subsequent diiron intermediates in the presence of substrate. (4) Thr-201 may have a role in proton delivery during the transition between diiron intermediates (*44*). It is feasible that protonation of the bound peroxide will help to control its reactivity with the diiron center. Heterolytic cleavage of the peroxodiferric O−O bond likely requires asymmetric protonation (*44*). One role of Thr-201 may be to prevent asymmetric protonation prior to substrate binding to retain the peroxo species at the active site. The removal of Thr-201 would allow faster protonation and formation of the subsequent intermediates through the intermediacy of active site water or other residues.

CONCLUSION

This work has provided evidence of the participation of Thr-201 in the diiron monooxygenase reaction cycle. Through stabilization of a peroxo-level intermediate, we propose that T201 T4moH serves to maintain coupling of the enzyme reaction even as substrate concentrations fall below saturating levels. The catalytic efficiency afforded by this otherwise nonessential residue may serve to explain why Thr-201 is conserved among the diiron monooxygenases.

ACKNOWLEDGMENT

We thank Dr. George N. Phillips, Jr., Dr. Jason G. McCoy, and Dr. Craig A. Bingman (University of Wisconsin) for access to crystallography equipment and many useful discussions.

SUPPORTING INFORMATION AVAILABLE

Crystallography statistics (Table S1), stereo image of helix αE in T201 and T201A overlaid (Figure S1), and stereo image comparing positions of T4moH diiron center ligands E197 and E231 in different structures (Figure S2). This material is available free of charge via the Internet at http://pubs.acs.org.

REFERENCES

1. Wallar, B. J., and Lipscomb, J. D. (1996) Dioxygen activation by enzymes containing binuclear non-heme iron clusters. *Chem. Rev. 96*, 2625–2658.
2. Fox, B. G. (1998) Catalysis by non-heme iron-containing enzymes. In *Comprehensive Biological Catalysis* (Sinnott, M., Ed.) pp 261−348, Academic Press, London.
3. Leahy, J. G., Batchelor, P. J., and Morcomb, S. M. (2003) Evolution of the soluble diiron monooxygenases. *FEMS Microbiol. Rev. 27*, 449–479.
4. Fox, B. G., Surerus, K. K., Munck, E., and Lipscomb, J. D. (1988) Evidence for a μ-oxo-bridged binuclear iron cluster in the hydroxylase component of methane monooxygenase. *J. Biol. Chem. 263*, 10553–10556.
5. Pikus, J. D., Studts, J. M., Achim, C., Kauffmann, K. E., Münck, E., Steffan, R. J., McClay, K., and Fox, B. G. (1996) Recombinant toluene 4-monooxygenase: Catalytic and Mössbauer studies of the purified diiron and Rieske components of a four-protein complex. *Biochemistry 35*, 9106–9119.
6. Murray, L. J., and Lippard, S. J. (2007) Substrate trafficking and dioxygen activation in bacterial multicomponent monooxygenases. *Acc. Chem. Res. 40*, 466–474.
7. Lipscomb, J. D. (1994) Biochemistry of the soluble methane monooxygenase. *Annu. Rev. Microbiol. 48*, 371–399.
8. Lippard, S. J. (2005) Hydroxylation of C-H bonds at carboxylate-bridged diiron centers. *Philos. Trans. R. Soc. London, Ser. A 363*, 861–877.
9. Fox, B. G., Froland, W. A., Dege, J. E., and Lipscomb, J. D. (1989) Methane monooxygenase from *Methylosinus trichosporium* OB3b. Purification and properties of a three-component system with high specific activity from a type II methanotroph. *J. Biol. Chem. 264*, 10023–10033.
10. Lee, S. K., Nesheim, J. C., and Lipscomb, J. D. (1993) Transient intermediates of the methane monooxygenase catalytic cycle. *J. Biol. Chem. 268*, 21569–21577.
11. Liu, K. E., Valentine, A. M., Wang, D., Huynh, B. H., Edmondson, D. E., Salifoglou, A., and Lippard, S. J. (1995) Kinetic and spectroscopic characterization of intermediates and component interactions in reactions of methane monooxygenase from *Methylococcus capsulatus* (Bath). *J. Am. Chem. Soc. 117*, 10174–10185.
12. Lee, S. K., Fox, B. G., Froland, W. A., Lipscomb, J. D., and Munck, E. (1993) A transient intermediate of the methane monooxygenase catalytic cycle containing an $Fe^{IV}Fe^{IV}$ cluster. *J. Am. Chem. Soc. 115*, 6450–6451.
13. Yun, D., Garcia-Serres, R., Chicalese, B. M., An, Y. H., Huynh, B. H., and Bollinger, J. M. (2007) (μ-1,2-Peroxo)diiron(III/III) complex as a precursor to the diiron(III/IV) intermediate X in the assembly of the iron-radical cofactor of ribonucleotide reductase from mouse. *Biochemistry 46*, 1925–1932.
14. Jameson, G. N., Jin, W., Krebs, C., Perreira, A. S., Tavares, P., Liu, X., Theil, E. C., and Huynh, B. H. (2002) Stoichiometric production of hydrogen peroxide and parallel formation of ferric multimers through decay of the diferric-peroxo complex, the first detectable intermediate in ferritin mineralization. *Biochemistry 41*, 13435–13443.
15. Broadwater, J. A., Ai, J., Loehr, T. M., Sanders-Loehr, J., and Fox, B. G. (1998) Peroxodiferric intermediate of stearoyl-acyl carrier protein Δ9 desaturase: Oxidase reactivity during single turnover and implications for the mechanism of desaturation. *Biochemistry 37*, 14664–14671.
16. Ruzicka, F., Huang, D. S., Donnelly, M. I., and Frey, P. A. (1990) Methane monooxygenase catalyzed oxygenation of 1,1-dimethylcyclopropane. Evidence for radical and carbocationic intermediates. *Biochemistry 29*, 1696–1700.
17. Jin, Y., and Lipscomb, J. D. (1999) Probing the mechanism of C-H activation: Oxidation of methylcubane by soluble methane monooxygenase from *Methylosinus trichosporium* OB3b. *Biochemistry 38*, 6178–6186.
18. Moe, L. A., Hu, Z., Deng, D., Austin, R. N., Groves, J. T., and Fox, B. G. (2004) Remarkable aliphatic hydroxylation by the diiron enzyme toluene 4-monooxygenase in reactions with radical or cation diagnostic probes norcarane, 1,1-dimethylcyclopropane, and 1,1-diethylcyclopropane. *Biochemistry 43*, 15688–15701.

19. Valentine, A. M., LeTadic-Biadatti, M. H., Toy, P. H., Newcomb, M., and Lippard, S. J. (1999) Oxidation of ultrafast radical clock substrate probes by the soluble methane monooxygenase from *Methylococcus capsulatus* (Bath). *J. Biol. Chem. 274*, 10771–10776.
20. Mitchell, K. H., Rogge, C. E., Gierahn, T., and Fox, B. G. (2003) Insight into the mechanism of aromatic hydroxylation by toluene 4-monooxygenase by use of specifically deuterated toluene and p-xylene. *Proc. Natl. Acad. Sci. U.S.A. 100*, 3784–3789.
21. Murray, L. J., Naik, S. G., Ortillo, D. O., Garcia-Serres, R., Lee, J. K., Huynh, B. H., and Lippard, S. J. (2007) Characterization of the arene-oxidizing intermediate in ToMOH as a diiron(III) species. *J. Am. Chem. Soc. 129*, 14500–14510.
22. Pikus, J. D., Mitchell, K. H., Studts, J. M., McClay, K., Steffan, R. J., and Fox, B. G. (2000) Threonine 201 in the diiron enzyme toluene 4-monooxygenase is not required for catalysis. *Biochemistry 39*, 791–799.
23. Murray, L. J., Garcia-Serres, R., Naik, S., Huynh, B. H., and Lippard, S. J. (2006) Dioxygen activation at non-heme diiron centers: Characterization of intermediates in a mutant form of toluene/o-xylene monooxygenase hydroxylase. *J. Am. Chem. Soc. 128*, 7458–7459.
24. Hemmi, H., Studts, J. M., Chae, Y. K., Song, J., Markley, J. L., and Fox, B. G. (2001) Solution structure of the toluene 4-monooxygenase effector protein (T4moD). *Biochemistry 40*, 3512–3524.
25. Elsen, N. L., Moe, L. A., McMartin, L. A., and Fox, B. G. (2007) Redox and functional analysis of the Rieske ferredoxin component of the toluene 4-monooxygenase. *Biochemistry 46*, 976–986.
26. Bailey, L. J., Elsen, N. L., Pierce, B. S., and Fox, B. G. (2008) Soluble expression and purification of the oxidoreductase component of toluene 4-monooxygenase. *Protein Expression Purif. 57*, 9–16.
27. Bailey, L. J., McCoy, J. G., Phillips, G. N.Jr., and Fox, B. G. (2008) Structural consequences of effector protein complex formation in a diiron hydroxylase. *Proc. Natl. Acad. Sci. U.S.A. 105*, 19194–19198.
28. Mitchell, K. H., Studts, J. M., and Fox, B. G. (2002) Combined participation of effector protein binding and hydroxylase active site residues provide toluene 4-monooxygenase regiospecificity. *Biochemistry 41*, 3176–3188.
29. Whittaker, J. W., Orville, A. M., and Lipscomb, J. D. (1990) Protocatechuate 3,4-dioxygenase from *Brevibacterium fuscum*. *Methods Enzymol. 188*, 82–88.
30. Yang, X., and Ma, K. (2005) Determination of hydrogen peroxide generated by reduced nicotinamide adenine dinucleotide oxidase. *Anal. Biochem. 344*, 130–134.
31. Otwinowski, Z., and Minor, W. (1997) The processing of X-ray difrraction data collected in oscillation mode. *Methods Enzymol. 276*, 307–326.
32. Vagin, A., and Teplyakov, A. (1997) MOLREP: An automated program for molecular replacement. *J. Appl. Crystallogr. 30*, 1022–1025.
33. Adams, P. D., Grosse-Kunstleve, R. W., Hung, L. W., Ioerger, T. R., McCoy, A. J., Moriarty, N. W., Read, R. J., Sacchettini, J. C., Sauter, N. K., and Terwilliger, T. C. (2002) PHENIX: Building new software for automated crystallographic structure determination. *Acta Crystallogr. D58*, 1948–1954.
34. Emsley, P., and Cowtan, K. (2004) Coot: Model-building tools for molecular graphics. *Acta Crystallogr. D60*, 2126–2132.
35. Murshudov, G. N., Vagin, A. A., and Dodson, E. J. (1997) Refinement of macromolecular structures by the maximum-likelihood method. *Acta Crystallogr. D53*, 240–255.
36. Lovell, S. C., Davis, I. W., Arendall, W. B.III, de Bakker, P. I. W., Word, J. M., Prisant, M. G., Richardson, J. S., and Richardson, D. C. (2003) Structure validation by C-α geometry: ϕ, ψ and C-β deviation. *Proteins: Struct., Funct., Genet. 50*, 437–450.
37. DeLano, W. L. (2002) *The PyMOL Molecular Graphics System*, DeLano Scientific, San Carlos, CA.
38. Taylor, R. (1990) *Electrophilic Aromatic Substitution*, John Wiley & Sons, New York.
39. Newman, L. M., and Wackett, L. P. (1995) Purification and characterization of toluene 2-monooxygenase from *Burkeholderia cepacia* G4. *Biochemistry 34*, 14066–14076.
40. Switala, J., and Loewen, P. C. (2002) Diversity of properties among catalases. *Arch. Biochem. Biophys. 401*, 145–154.
41. Neibergall, M. B., Stubna, A., Mekmouche, Y., Munck, E., and Lipscomb, J. D. (2007) Hydrogen peroxide dependent cis-dihydroxylation of benzoate by fully oxidized benzoate 1,2-dioxygenase. *Biochemistry 46*, 8004–8016.
42. Guy, J. E., Abreu, I. A., Moche, M., Lindqvist, Y., Whittle, E., and Shanklin, J. (2006) A single mutation in the castor Δ9-18:0-desaturase changes reaction partitioning from desaturation to oxidase chemistry. *Proc. Natl. Acad. Sci. U.S.A. 103*, 17220–17224.
43. Raag, R., Martinis, S. A., Sligar, S. G., and Poulos, T. L. (1991) Crystal structure of the cytochrome P-450CAM active site mutant Thr252Ala. *Biochemistry 30*, 11420–11429.
44. Lee, S. K., and Lipscomb, J. D. (1999) Oxygen activation catalyzed by methane monooxygenase hydroxylase component: Proton delivery during the O-O bond cleavage steps. *Biochemistry 38*, 4423–4432.
45. Brazeau, B. J., Austin, R. N., Tarr, C., Groves, J. T., and Lipscomb, J. D. (2001) Intermediate Q from soluble methane monooxygenase hydroxylates the mechanistic substrate probe norcarane: Evidence for a stepwise reaction. *J. Am. Chem. Soc. 123*, 11831–11837.
46. Beauvais, L. G., and Lippard, S. J. (2005) Reactions of the peroxo intermediate of soluble methane monooxygenase hydroxylase with ethers. *J. Am. Chem. Soc. 127*, 7370–7378.
47. Andersson, M. E., Högbom, M., Rinaldo-Matthis, A., Andersson, K. K., Sjöberg, B.-M., and Nordlund, P. (1999) The crystal structure of an azide complex of the diferrous R2 subunit of ribonucleotide reductase displays a novel carboxylate shift with important mechanistic implications for diiron-catalyzed oxygen activation. *J. Am. Chem. Soc. 121*, 2346–2352.
48. Green, J., and Dalton, H. (1985) Protein B of soluble methane monooxygenase from *Methylococcus capsulatus* (Bath). *J. Biol. Chem. 260*, 15795–15801.
49. Poulos, T. L., and Raag, R. (1992) Cytochrome P450cam: Crystallography, oxygen activation, and electron transfer. *FASEB J. 6*, 674–679.
50. Kovaleva, E. G., and Lipscomb, J. D. (2008) Versatility of biological non-heme Fe(II) centers in oxygen activation reactions. *Nat. Chem. Biol. 4*, 186–193.
51. Schwartz, J. K., Wei, P. P., Mitchell, K. H., Fox, B. G., and Solomon, E. I. (2008) Geometric and electronic structure studies of the binuclear nonheme ferrous active site of toluene-4-monooxygenase: Parallels with methane monooxygenase and insight into the role of the effector proteins in O_2 activation. *J. Am. Chem. Soc. 130*, 7098–7109.